Inorganic Chemistry

Article

pubs.acs.org/IC

Formation of Soluble Hexanuclear Neptunium(IV) Nanoclusters in Aqueous Solution: Growth Termination of Actinide(IV) Hydrous Oxides by Carboxylates

Koichiro Takao,*[,†,‡] Shinobu Takao,[†,§] Andreas C. Scheinost,[†] Gert Bernhard,[†] and Christoph Hennig*[,†]

[†]Institute of Radiochemistry, Helmholtz Zentrum Dresden-Rossendorf, P.O. Box 51 01 19, 01314 Dresden, Germany

[‡]Department of Materials and Life Science, Seikei University, 3-3-1, Kichijoji-kitamachi, Musashino-shi, Tokyo 180-8633, Japan

[§]Innovation Research Center for Fuel Cells, The University of Electro-Communications, 1-5-1, Chofugaoka, Chofu-shi, Tokyo 182-8585, Japan

Supporting Information

ABSTRACT: Complexation of Np^{IV} with several carboxylates ($RCOO^-$; R = H, CH_3, or $CHR'NH_2$; R′ = H, CH_3, or CH_2SH) in moderately acidic aqueous solutions was studied by using UV−vis−NIR and X-ray absorption spectroscopy. As the pH increased, all investigated carboxylates initiated formation of water-soluble hexanuclear complexes, $Np_6(\mu\text{-}RCOO)_{12}(\mu_3\text{-}O)_4(\mu_3\text{-}OH)_4$, in which the neighboring Np atoms are connected by $RCOO^-$ *syn*−*syn* bridges and the triangular faces of the Np_6 octahedron are capped with $\mu_3\text{-}O^{2-}/\mu_3\text{-}OH^-$. The structure information of $Np_6(\mu\text{-}RCOO)_{12}(\mu_3\text{-}O)_4(\mu_3\text{-}OH)_4$ in aqueous solution was extracted from the extended X-ray absorption fine structure data: Np−O^{2-} = 2.22−2.23 Å (coordination number N = 1.9−2.2), Np−O($RCOO^-$) and Np−OH^- = 2.42−2.43 Å (N = 5.6−6.7 in total), Np···C($RCOO^-$) = 3.43 Å (N = 3.3−3.9), Np···Np(neighbor) = 3.80−3.82 Å (N = 3.6−4.0), and Np···Np(terminal) = 5.39−5.41 Å (N = 1.0−1.2). For the simpler carboxylates, the gross stability constants of $Np_6(\mu\text{-}RCOO)_{12}(\mu_3\text{-}O)_4(\mu_3\text{-}OH)_4$ and related monomers, $Np(RCOO)(OH)_2^+$, were determined from the UV−vis−NIR titration data: when R = H, $\log \beta_{6,12,-12} = 42.7 \pm 1.2$ and $\log \beta_{1,1,-2} = 2.51 \pm 0.05$ at I = 0.62 M and 295 K; when R = CH_3, $\log \beta_{6,12,-12} = 52.0 \pm 0.7$ and $\log \beta_{1,1,-2} = 3.86 \pm 0.03$ at I = 0.66 M and 295 K.

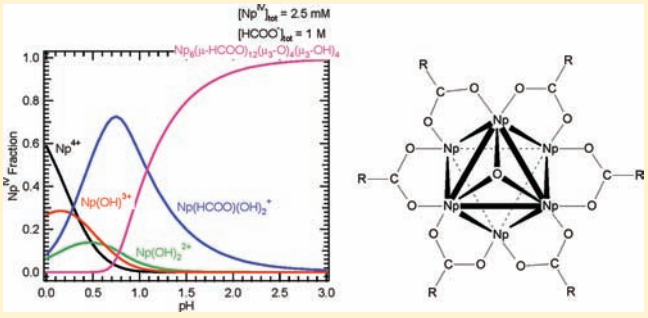

1. INTRODUCTION

The actinide elements comprise a family of f-elements together with lanthanides. However, the wider variety of oxidation states of the actinides differentiates them from lanthanides. Actinide(III) and actinide(IV) form spherical ions, M^{3+} and M^{4+}, respectively. Therefore, the coordination is not restricted in space, leading to the diversity of their coordination chemistry. The number of coordination sites around M^{3+} and M^{4+} varies from 6 to 10.[1,2]

Considering environmental aspects, the +4 oxidation state is more important than the +3 state, because the former is commonly found in Th, U, Np, and Pu as a stable oxidation state.[3] As a common characteristic, tetravalent actinides show a strong tendency toward hydrolysis, thereby producing mono- and polynuclear hydrolyzed species [e.g., $M(OH)_n^{4-n}$, $M_4(OH)_{12}^{4+}$, and $M_6(OH)_{15}^{9+}$] and colloids and/or precipitates of actinide(IV) hydrous oxides.[4] The solubility and aqueous speciation of actinide(IV) are particularly interesting for the storage of nuclear waste underground for predicting their potential mobility or immobility.[5]

In geomedia, many kinds of organic and inorganic compounds are present, which are able to interact with the radionuclides. Among them, carboxylates ($RCOO^-$) comprise a large group of typical organic ligands and form stable complexes with various M^{n+} ions. The resulting carboxylato complexes are often highly soluble in aqueous media and, therefore, might release the radiotoxic elements from the waste repository to the environment. Humic and fulvic acid fractions of natural organic matter, which also contains carboxylic groups, play an important role in the binding of M^{n+} in soils and groundwater. Furthermore, the carboxylic group is commonly found in proteins and peptides as an amino acid residue (glutamate and aspartate) and C-terminal group and may have key functionalities in the interaction with M^{n+}.[6]

Several solid compounds of actinide(IV) carboxylates were reviewed by Casellato et al.[7] According to this review and references cited therein, Th^{IV} and U^{IV} are polymerized by $HCOO^-$ and CH_3COO^- bridges in a *syn*−*syn* coordination manner, resulting in an infinite one-dimensional metal−organic chain. Ternary actinide(IV) complexes with CH_3COO^- and OH^- have also been found. Although correct atomic

Received: July 12, 2011
Published: January 5, 2012

   dx.doi.org/10.1021/ic201482n | *Inorg. Chem.* 2012, 51, 1336−1344

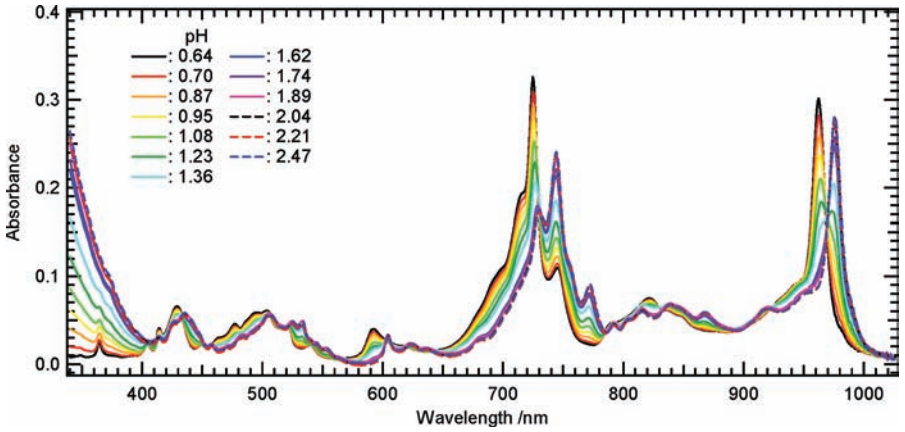

Figure 1. UV−vis−NIR absorption spectra of Np^{IV} (2.50×10^{-3} M) with 1.00 M $HCOO^-$/HCOOH at I = 0.62 M $(H,NH_4)ClO_4$ and different pH values.

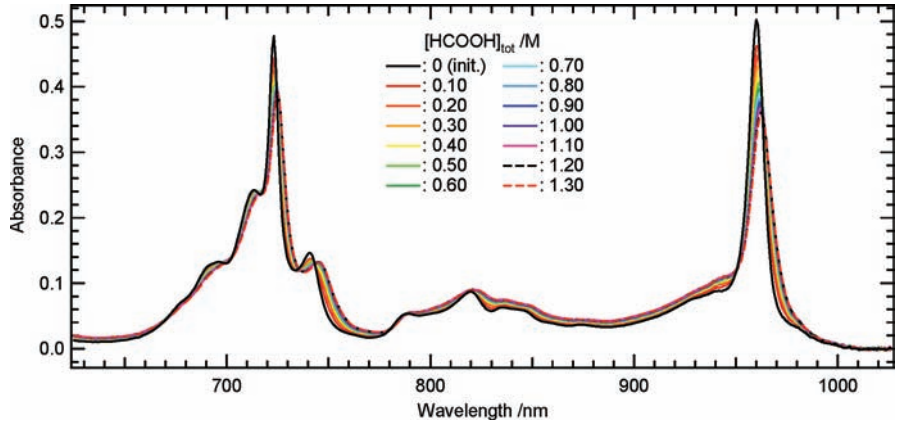

Figure 2. UV−vis−NIR absorption spectra of Np^{IV} (3.10×10^{-3} M) at pH 0.59, I = 0.62 M $(H,NH_4)ClO_4$, and different total HCOOH concentrations ($[HCOO^-]_{tot}$).

configurations in those compounds have not been determined, several potential polymeric structures with OH^- and/or CH_3COO^- bridges were hypothetically proposed. The infinite "$-(RCOO\text{-}M^{4+})_n-$" chain of the reported solid compounds hardly occurs in solution and can form only during the crystallization process. If the bridging character of $RCOO^-$ toward actinide(IV) appears in the aqueous solution, a discrete polynuclear actinide(IV) cluster could be formed as a soluble species. On one hand, previous potentiometric titration studies of complexation of Th^{IV} with several $RCOO^-$ groups did not assume any possibility of such polynucleation.[8] Furthermore, several carboxylato complexes of Np^{IV} in aqueous solution were reported, but only the monomeric species were taken into account.[9] On the other hand, Toraishi et al. recently investigated a Th^{IV}−glycolate aqueous system by combining potentiometry, ^{13}C NMR, and extended X-ray absorption fine structure (EXAFS) spectroscopy and suggested formation of "cubane-like" tetranuclear Th^{IV}−glycolate complexes.[10] Very recently, we isolated several hexanuclear complexes of Th^{IV} and U^{IV}, $M_6(\mu\text{-}HCOO)_{12}(\mu_3\text{-}O)_4(\mu_3\text{-}OH)_4(L)_6$ (M = Th or U; L = H_2O or CH_3OH), from aqueous solutions and determined their structures by means of single-crystal X-ray diffraction.[11a] The pH dependence of an EXAFS spectrum of U^{IV} with $HCOO^-$/HCOOH indicated that the hexanuclear nanosized cluster is formed as a soluble species in aqueous solution with a predominant presence at pH >2.3. The EXAFS investigation of the analogue Th^{IV}−$HCOO^-$ system revealed a lower stability of the Th^{IV} hexamer. This difference is related to the weaker propensity of Th^{IV} for hydrolysis compared to that of U^{IV}, because the μ_3-O(H) groups arising from hydrolysis of M^{4+} play a very important role in the construction of the M^{IV}_6 octahedron by connecting three neighboring M^{4+} ions and capping each face of this polyhedron. The very similar Th^{IV} hexamers with several kinds of $RCOO^-$ groups were also isolated by Knope et al.[11b] Several related hexanuclear U^{IV} complexes, bearing bridging ligands other than $RCOO^-$, were also reported.[12]

With an increasing atomic number, the hydrolysis of actinide(IV) tends to become stronger.[4] Therefore, we assumed that Np^{IV} and Pu^{IV} may form more stable hexanuclear clusters through their hydrolysis and the *syn*−*syn* bridging by $RCOO^-$ in aqueous solution. In this study, we investigated complexation of Np^{IV} with several carboxylate-based ligands ($HCOO^-$, CH_3COO^-, glycine, L-alanine, and L-cysteine) in aqueous solution by means of UV−vis−NIR absorption and EXAFS spectroscopy. In particular, the latter technique can provide structural evidence of the potential formation of polynuclear species in solution.

2. RESULTS AND DISCUSSION

2.1. UV−Vis−NIR Absorption Spectroscopy. UV−vis−NIR absorption spectra of Np^{IV} (2.50×10^{-3} M) with 1.00 M $HCOO^-$/HCOOH at I = 0.62 M $(H,NH_4)ClO_4$ and different pH values are shown in Figure 1. For the sake of clarity,

dx.doi.org/10.1021/ic201482n | Inorg. Chem. 2012, 51, 1336−1344

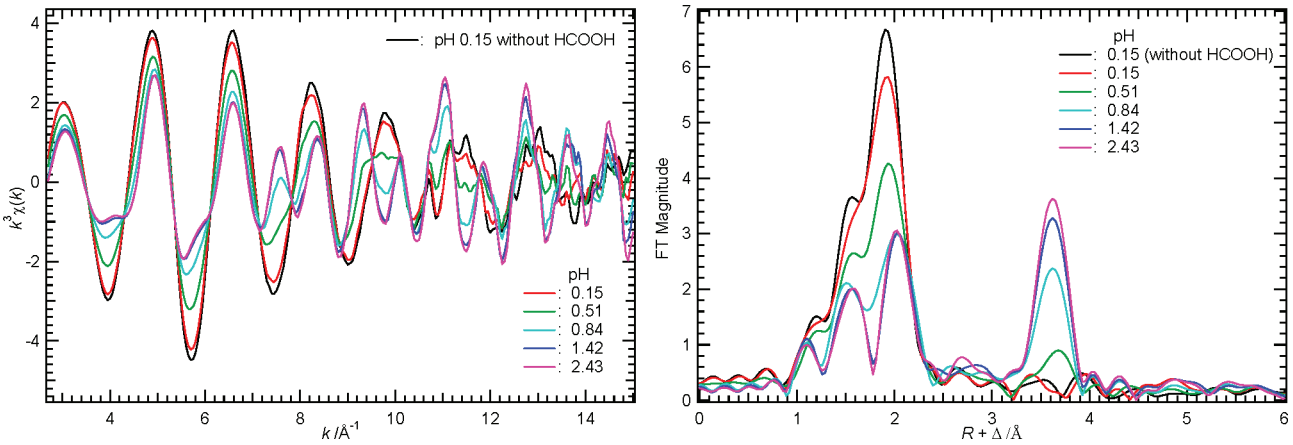

Figure 3. k^3-weighted Np L_{III}-edge EXAFS spectra (left) and their FTs (right) of Np^{IV} (2.5×10^{-2} M) with 1.00 M $HCOO^-$/HCOOH at I = 0.62 M $(H,NH_4)ClO_4$ at various pH values.

magnified sections are displayed in Figure S1 of the Supporting Information. The spectra show the characteristic features of Np^{IV}, strong absorption bands around 590, 730, 820, and 960 nm and fine structure from 400 to 550 nm.[13] Systematic spectral changes were observed with increasing pH values. Furthermore, isosbestic points were found at 412, 433, 451, 456, 506, 522, 560, 603, 607, 619, 642, 729, 785, 830, 899, 923, and 969 nm. This means that one equilibrium is predominant under the experimental conditions described in the legend of Figure 1. At pH >2, the spectral change with pH variation converges, indicating the product of the equilibrium reaction is completely formed. Even at the lowest pH, the absorption spectrum in the presence of HCOOH is different from that in the absence of HCOOH at the same pH as shown in Figure S2 of the Supporting Information. Thus, all the Np^{IV} species present in Figure 1 form complexes with $HCOO^-$.

Prior to a discussion of the details of the equilibrium detected in Figure 1, it is necessary to examine what species occurs at the lowest pH. For that purpose, a second experiment was performed at a constant pH with systematic variation of the total $HCOO^-$ concentration, $[HCOO^-]_{tot}$. Figure 2 and Figure S3 of the Supporting Information display the UV−vis−NIR absorption spectra of Np^{IV} (3.10×10^{-3} M) at pH 0.59, I = 0.62 M $(H,NH_4)ClO_4$, and different $[HCOO^-]_{tot}$ values. As shown in the latter figure, the spectrum varies slightly with increasing $[HCOO^-]_{tot}$ values in the range from 350 to 650 nm. In contrast, the greater spectral changes with the clear isosbestic points at 670, 698, 703, 717, 725, 735, 743, 781, 950, and 963 nm were observed around 720 and 960 nm. The presence of the isosbestic points indicates only one equilibrium reaction different from that observed in Figure 1. Furthermore, the spectral changes ceased at $[HCOO^-]_{tot} \geq 1.00$ M. The final spectrum is identical to that at the lowest pH in Figure 1, indicating that the same initial species as in Figure 1 was formed.

A series of UV−vis−NIR absorption spectra of Np^{IV} (2.39×10^{-3} M) with 1.00 M CH_3COO^-/CH_3COOH at I = 0.66 M $(H,NH_4)ClO_4$ and different pH values exhibits a trend similar to that observed in the Np^{IV}−$HCOO^-$ system. The obtained spectral series as a function of pH is displayed in Figure S4 of the Supporting Information. The characteristic features of Np^{IV} were also identified in all the spectra recorded here, i.e., the strong absorption bands around 590, 700, 820, and 960 nm and fine structure from 400 to 550 nm. Even at pH 0.52, the absorption spectrum is different from that of Np^{IV} in the absence of CH_3COO^-/CH_3COOH, indicating the formation of a complex of Np^{4+} with CH_3COO^-. This reaction, however, seems not to be completed at the lowest pH examined, because the shoulder at 960 nm arising from Np^{IV} not coordinated by CH_3COO^- was also observed. The isosbestic points can be found at 602, 731, and 970 nm at pH >1.00. With an increasing pH, the same trend as that in Figure 1 was observed. In particular, the spectra at pH >2.95 are quite similar to that at the highest pH in Figure 1, suggesting that the analogous Np^{IV} species is also formed in this system. UV−vis−NIR titration at a constant pH and systematic variation of the total CH_3COO^- concentration, $[CH_3COO^-]_{tot}$, have been conducted, and the result is shown in Figure S5 of the Supporting Information [$[Np^{IV}]_{tot} = 2.93 \times 10^{-3}$ M at pH 0.54 and I = 0.66 M $(H,NH_4)ClO_4$]. With clear isosbestic points at 696, 705, 726, 736, 745, 781, 792, and 965 nm, the dependence on ligand concentration was observed in a manner similar to that depicted in Figure 2 and Figure S3 of the Supporting Information. The presence of the isosbestic points indicates only one equilibrium reaction different from that observed in Figure S4 of the Supporting Information. The spectral changes converged at $[CH_3COO^-]_{tot} > 1.00$ M. In summary, we have observed the formation of two kinds of Np^{IV}−$RCOO^-$ complexes (R = H or CH_3) in the UV−vis−NIR experiments. The strong hydrolysis character of Np^{IV} should be taken into account here. However, NpO_2 colloid formation can be excluded, because the integral baseline intensity remained unchanged.. Therefore, soluble ternary complexes of Np^{IV} with $RCOO^-$ and OH^- occur even under the weakly basic condition in both systems; i.e., growing of the colloidal NpO_2 particle was prevented by $RCOO^-$.

To obtain an overview of the species distribution for the spectral series in Figure 1 and Figure S4 of the Supporting Information, we performed principal component analysis (PCA).[14] As a result, very low eigenvalues of $<10^{-1}$ were obtained for third and later principal components in each spectral series, which were negligibly smaller than those of first and second components. This means that each spectral series of Figure 1 and Figure S4 of the Supporting Information is governed by two major components, being in agreement with the occurrence of the isosbestic points that indicate the presence of a single equilibrium during the experiment. It should also be emphasized that the spectral changes that cease

dx.doi.org/10.1021/ic201482n | Inorg. Chem. 2012, 51, 1336−1344

with increasing pH values in both Figure 1 and Figure S4 of the Supporting Information strongly indicate that the single product of the equilibrium is predominantly formed under the high-pH conditions (>2.0 when R = H and >3.0 when R = CH_3).

2.2. EXAFS Spectroscopy. To identify the Np^{IV}–$HCOO^-$ complexes in the solution, Np L_{III}-edge EXAFS spectra of Np^{IV} (2.5×10^{-2} M) with 1.00 M $HCOO^-$/HCOOH at I = 0.62 M $(H,NH_4)ClO_4$ at various pH values were recorded. The k^3-weighted EXAFS spectra (k space) and their Fourier transforms (R space) are shown in Figure 3. This figure also contains the reference spectrum recorded in the absence of HCOOH at pH 0.15. In k space, the low-frequency EXAFS oscillation in the range from 3 to 7 $Å^{-1}$ decreases with an increasing pH, resulting in a decrease and splitting of the peak around $R + \Delta = 2$ Å in R space. At $k > 7$ $Å^{-1}$, a high-frequency oscillation appears, corresponding to the growth of the peak at $R + \Delta = 3.6$ Å in R space. This strong peak is supposed to arise from the contribution of very heavy atoms surrounding the excited Np, implying formation of a Np^{IV} polynuclear species. At pH 0.15, such a peak is not detected, indicating that Np^{IV} exclusively stays in a monomeric form. Taking the result of the UV–vis–NIR experiments into account, we can assign the equilibrium observed in Figure 1 to the formation of Np^{IV} polynuclear species. As shown in the UV–vis–NIR absorption spectra of the EXAFS samples (Figure S6 of the Supporting Information), it must be emphasized that the formation of the final Np^{IV}–$HCOO^-$ species in the more concentrated Np^{IV} system (EXAFS; $[Np^{IV}]_{tot} = 2.5 \times 10^{-2}$ M) is more significant than that in the less concentrated system (UV–vis–NIR; $[Np^{IV}]_{tot} = 2.5 \times 10^{-3}$ M); e.g., the Np···Np interaction in the R space of Figure 3 is clearly observed at $[Np^{IV}]_{tot} = 2.5 \times 10^{-2}$ M and pH 0.84, whereas the starting species is still predominant at $[Np^{IV}]_{tot} = 2.5 \times 10^{-3}$ M and pH 0.87. Thus, $[Np^{IV}]_{tot}$ affects the stability of the final product. Recently, we isolated several hexanuclear clusters in analogue Th^{IV}– and U^{IV}–$HCOO^-$ complexes, $M_6(\mu\text{-}HCOO)_{12}(\mu_3\text{-}O)_4(\mu_3\text{-}OH)_4(L)_6$ (M^{IV} = Th^{4+} or U^{4+}; L = H_2O or CH_3OH), and confirmed their presence in moderately acidic aqueous solutions.[11a] The EXAFS spectrum of the sample at pH 2.43 shown in Figure 3 closely resembles that of solid $M_6(\mu\text{-}HCOO)_{12}(\mu_3\text{-}O)_4(\mu_3\text{-}OH)_4(H_2O)_6$ (M^{IV} = Th^{4+} or U^{4+}) whose molecular structures were determined by single-crystal X-ray diffraction. The extracted structural parameters from the EXAFS spectrum at pH 2.43 on the basis of the model structure of $Th_6(\mu\text{-}HCOO)_{12}(\mu_3\text{-}O)_4(\mu_3\text{-}OH)_4(H_2O)_6$ (Figure 4)[11a] are listed in Table 1. This table also contains the corresponding interatomic distances observed in the analogue Th^{IV} and U^{IV} hexamers in crystalline states. The best fit is shown in Figure S7 of the Supporting Information together with the experimental data. The Np^{IV}–$HCOO^-$ complex reveals four next-neighbor Np···Np_n distances of 3.81 Å and one terminal Np···Np_t distance of 5.40 Å, indicating the arrangement of six Np atoms in the corners of an octahedron. Each Np atom is coordinated by 2.1 O atoms at a Np–O distance of 2.23 Å and 6.3 O atoms at a distance of 2.43 Å. The shorter Np–O distance belongs to two μ_3-O^{2-} ions (O_O), whereas the longer Np–O distance comprises the scattering contribution of two μ_3-OH^- ions (O_{OH}) and four carboxylate O atoms directly bonded to Np (O_C) (Figure 4). The coordination numbers estimated by the EXAFS curve fit involve an uncertainty of ~10%, which is sufficiently low for identification of the hexanulcear Np^{IV} complex, $Np_6(\mu\text{-}HCOO)_{12}(\mu_3\text{-}O)_4(\mu_3\text{-}OH)_4$,

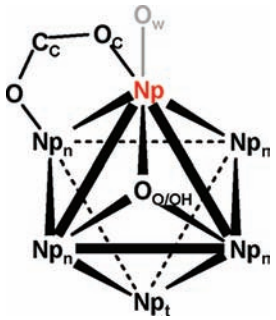

Figure 4. Structural model for the EXAFS curve fit imported from the crystal structure of $Th_6(\mu\text{-}HCOO)_{12}(\mu_3\text{-}O)_4(\mu_3\text{-}OH)_4(H_2O)_6$.[11] Np (red) is assumed to be the X-ray-absorbing atom in the EXAFS experiment (note that all the Np atoms are equivalent). Although each pair of two vicinal Np atoms is bridged by the carboxylate (O_C–C_C–O), only one is shown here for the sake of clarity. All the Np_3 sets in the triangular faces are connected by μ_3-O/OH ($O_{O/OH}$). The O atom of the terminal H_2O (O_w) was not involved in the current fit (see the text).

by taking into account the similarity in the chemical behavior of the actinide(IV) ions and the stronger tendency of the formation of the final product toward more $[Np^{IV}]_{tot}$.

In the structure of $Np_6(\mu\text{-}HCOO)_{12}(\mu_3\text{-}O)_4(\mu_3\text{-}OH)_4$ (Figure 4), it is noteworthy that all the Np atoms in this Np_6 octahedron are equivalent. Each pair of two vicinal Np atoms is connected by *syn–syn* bridging of $HCOO^-$. Furthermore, μ_3-O/OH connects three Np atoms, forming the triangular face of an octahedron. The interatomic distances of the direct bonds ($Np–O_{O/OH/C}$) are in agreement with but slightly shorter than the corresponding distances in the solid Th^{IV}– and U^{IV}–$HCOO^-$ hexamers. This shortening results from the contraction of the actinide ionic radius. The presence of the capping H_2O molecules [O_w (Figure 4)] on each vertex of the M_6 octahedron, which was found in the solid Th^{IV} and U^{IV} hexamers, could not be confirmed because the single $M–O_w$ distances in the Th^{IV} and U^{IV} hexamer crystals scatter in the relatively wide range from 2.67 to 2.91 Å and it is difficult to distinguish the $Np–O_w$ contribution from the neighboring peak tailings of the much stronger $Np–O_{OH/C}$ scattering contribution, especially in the case of structural disorder. According to the crystal structures of the Th^{IV} and U^{IV} hexamers,[11] the $M–O_O$ distance is shorter than the $M–O_{OH}$ distance by ~0.2 Å, which is sufficiently large to be distinguished in EXAFS. Therefore, it is feasible to determine the degree of protonation on the μ_3-oxygen atom connecting three metal centers as discussed above. This suggests that the existing Np^{IV} hexamer is the noncharged complex, $Np_6(\mu\text{-}HCOO)_{12}(\mu_3\text{-}O)_4(\mu_3\text{-}OH)_4$, which is very similar to the previously descrived Th^{IV} and U^{IV} hexamers.[11,12] To reach a uniform charge distribution in the complex, four μ_3-O^{2-} and four μ_3-OH^- groups could be placed in S_4 symmetry.[11b] If the protonation to μ_3-O and deprotonation from μ_3-OH take place, the electronic energy states of the hexanuclear complex would be affected. As a result, further pH dependence would be observed in the UV–vis–NIR absorption spectrum series of Figure 1. Consequently, isosbestic points would never arise because of the additional equilibria. However, the actual UV–vis–NIR absorption spectra in Figure 1 show the isosbestic points, and the species detected by EXAFS is only $Np_6(\mu\text{-}HCOO)_{12}(\mu_3\text{-}O)_4(\mu_3\text{-}OH)_4$, suggesting that no protonation–deprotonation processes are present at least in the studied system. This suggestion may be

dx.doi.org/10.1021/ic201482n | Inorg. Chem. 2012, 51, 1336–1344

Table 1. Structural Parameters from a Curve Fit for $Np_6(\mu\text{-RCOO})_{12}(\mu_3\text{-O})_4(\mu_3\text{-OH})_4$ [R = H (Figure 3) at pH 2.43; R = CH_3 (Figure S7) at pH 3.02] and Corresponding Interatomic Distances in Crystalline Th^{IV} and U^{IV} Hexamers[a]

	R = H			R = CH_3				R_{cryst} (Å)[c]	
shell[b]	N	R (Å)	σ^2 (Å^2)	N	R (Å)	σ^2 (Å^2)	N_{cryst}[c]	Th^{IV}	U^{IV}
O_O	2.1	2.23	0.0046	1.9	2.22	0.0056	2	2.28	2.23
O_C/O_{OH}	6.3	2.43	0.0073	5.6	2.43	0.0076	6	2.50	2.44
C_C	3.3	3.43	0.0060	3.6	3.43	0.0056	4	3.49	3.39
M_n[d]	4.0	3.81	0.0049	3.6	3.80	0.0055	4	3.91	3.82
M_t[d]	1.0	5.40	0.0049	1.0	5.39	0.0064	1	5.52	5.40
	$\Delta E_0 = -3.5$ eV; R-factor = 0.02046			$\Delta E_0 = -1.2$ eV; R-factor = 0.04975					

[a] σ^2, Debye–Waller factor; ΔE_0, threshold energy shift. [b] Atomic notation follows Figure 4. [c] Coordination number (N_{cryst}) and mean interatomic distance (R_{cryst}) in the crystalline Th^{IV} and U^{IV} hexamers in ref 11a. [d] M = Np, Th, or U.

corroborated by the similar skeleton of $M_6(\mu\text{-HCOO})_{12}(\mu_3\text{-O})_4(\mu_3\text{-OH})_4$ in the isolated Th^{IV} and U^{IV} hexanuclear analogues of which μ_3-O and μ_3-OH were distinguishable.[11] Connecting the single peak at the lowest pH in Figure 3 with the PCA result for UV–vis–NIR, the initial species at the lower pH should be monomeric, such as $Np(HCOO)_x(OH)_y^{4-x-y}$.

The resulting k^3-weighted EXAFS spectra and their FTs of Np^{IV} (4.0×10^{-2} M) with 1.00 M CH_3COO^- at pH 0.80 and 3.02 are shown in Figure S8 of the Supporting Information together with the reference sample at $[CH_3COO^-]_{tot} = 0$. As a result, it was found that the Np^{IV}–CH_3COO^- species at pH 0.80 is dominantly monomeric while that at pH 3.02 is exclusively polymeric because of the characteristic strong peak at $R + \Delta = 3.6$ Å arising from the Np···Np interaction. The EXAFS curve fit using the model structure of Figure 4 shows good agreement with the EXAFS spectrum at the higher pH (Figure S9 of the Supporting Information). These data confirm the formation of the hexameric complex similar to that found in the Np^{IV}–$HCOO^-$ system. The estimated structural parameters are summarized in Table 1. The N values of O_O and $O_{OH/C}$ shells are 1.9 and 5.6, respectively, being again indicative of the formation of the noncharged $Np_6(\mu\text{-}CH_3COO)_{12}(\mu_3\text{-O})_4(\mu_3\text{-OH})_4$. The interatomic distance of each shell is slightly shorter than the corresponding distances in the crystalline Th^{IV}– and U^{IV}–$HCOO^-$ hexamers in a manner similar to that of $Np_6(\mu\text{-HCOO})_{12}(\mu_3\text{-O})_4(\mu_3\text{-OH})_4$.

In summary, it has been clarified here that the pH dependence of UV–vis–NIR and EXAFS spectra arises from an equilibrium between $Np(RCOO)_x(OH)_y^{4-x-y}$ and $Np_6(\mu\text{-}CH_3COO)_{12}(\mu_3\text{-O})_4(\mu_3\text{-OH})_4$ in both systems when R = H and CH_3.

2.3. Equilibrium Analysis. As mentioned above, Np^{IV} forms a monomeric complex with $RCOO^-$ at the lowest pH of Figures 1 and 3 and Figures S4 and S5 of the Supporting Information, and the hydrolysis of Np^{IV} should also be taken into consideration. In the pH series (Figure 1), the initial species seems to be a ternary monomeric complex consisting of Np^{IV}, $RCOO^-$, and OH^-, and the final product is $Np_6(\mu\text{-RCOO})_{12}(\mu_3\text{-O})_4(\mu_3\text{-OH})_4$. Therefore, the following general expression can be formulated.

$$6Np(RCOO)_x(OH)_y^{4-x-y} + (12 - 6x)\,RCOO^- + (8 - 6y)H_2O = Np_6(\mu\text{-RCOO})_{12}(\mu_3\text{-O})_4(\mu_3\text{-OH})_4 + (12 - 6y)H^+ \quad (1)$$

Both the numbers of $RCOO^-$ (x) and OH^- (y) groups in the starting Np^{IV}–$RCOO^-$ monomeric species may reach integers up to 2, because the molar ratio of $RCOO^-$ to Np^{4+} is 2 in the hexameric product, and the main hydrolysis products of Np^{IV} in the absence of $RCOO^-$ are $Np(OH)^{3+}$ and $Np(OH)_2^{2+}$.[4b,c] When R = H, the logarithmic equilibrium constants of eq 1 with $x = 1$ and different values of y were calculated as 13.3 ± 3.8 ($y = 0$), 20.4 ± 1.6 ($y = 1$), and 27.6 ± 0.9 ($y = 2$) from the absorbance (A) at 725 nm in Figure 1. When R = CH_3, this quantity was 4.2 ± 6.3, 16.5 ± 3.1, and 28.8 ± 0.5 for $y = 0$, 1, and 2, respectively. For $x = 2$, i.e., monomeric species of $Np(RCOO)_2(OH)_y^+$, much more significant uncertainty on the equilibrium constant of eq 1 was afforded. Consequently, the best reproducibility for the experiment makes $x = 1$ and $y = 2$ most plausible. Therefore, the existence of $Np(RCOO)(OH)_2^+$ at the lowest pH in Figures 1 and 3 and Figures S4 and S5 of the Supporting Information is most likely.

In the next step, we considered the formation of $Np(RCOO)(OH)_2^+$ (eq 2).

$$Np^{4+} + RCOO^- + 2H_2O = Np(RCOO)(OH)_2^+ + 2H^+ \quad (2)$$

Under the experimental conditions used for Figure 2, the absorbance A can be described as a function of $[HCOO^-]_{tot}$, which follows eq S8 (Supporting Information). The logarithmic gross stability constant of $Np(HCOO)(OH)_2^+$ ($\log \beta_{1,1,-2}$) estimated from A at 723 and 960 nm, where the maximal deviations through the experimental course were found, is 2.51 ± 0.05 (the detailed parameters of eq S8 are given in Table S1 of the Supporting Information). The $\log \beta_{1,1,-2}$ of $Np(CH_3COO)(OH)_2^+$ was also determined to be 3.86 ± 0.03 by the same procedure. Now, the formation of $Np_6(\mu\text{-RCOO})_{12}(\mu_3\text{-O})_4(\mu_3\text{-OH})_4$ can be written by eq 3.

$$6Np^{4+} + 12RCOO^- + 8H_2O = Np_6(\mu\text{-RCOO})_{12}(\mu_3\text{-O})_4(\mu_3\text{-OH})_4 + 12H^+ \quad (3)$$

The logarithmic gross stability constants of $Np_6(\mu\text{-RCOO})_{12}(\mu_3\text{-O})_4(\mu_3\text{-OH})_4$ ($\log \beta_{6,12,-12}$) for R = H and CH_3 are evaluated as 42.7 ± 1.2 and 52.0 ± 0.7, respectively. The summary of the related stability constants is given in Table 2. Using these stability constants, the speciation diagrams of the Np^{IV}–$RCOO^-$ systems under the experimental conditions of UV–vis–NIR (Figure 1 and Figure S4 of the Supporting Information) and EXAFS (Figure 3 and Figure S8 of the Supporting Information) have been calculated and are shown in Figures 5 and 6, respectively. At pH 0.64 in Figure 5a, the point at which the UV–vis–NIR titration experiment of Figure 1

dx.doi.org/10.1021/ic201482n | Inorg. Chem. 2012, 51, 1336–1344

Table 2. Gross Stability Constants ($\beta_{l,m,n}$) of Np^{IV}–$RCOO^-$ Complexes and Related Species

	stoichiometry				log $\beta_{l,m,n}$
R	Np^{4+} (l)	$RCOO^-$ (m)	H^+ (n)	product	I = 0.62 M (R = H), I = 0.66 M (R = CH_3)
–	1	0	−1	$Np(OH)^{3+}$	−0.343[a]
–	1	0	−2	$Np(OH)_2^{2+}$	−0.969[a]
H	0	1	1	HCOOH	3.376[a]
H	1	1	−2	$Np(HCOO)(OH)_2^+$	2.51 ± 0.05
H	6	12	−12	$Np_6(\mu\text{-}HCOO)_{12}(\mu_3\text{-}O)_4(\mu_3\text{-}OH)_4$	42.7 ± 1.2
CH_3	0	1	1	CH_3COOH	4.385[a]
CH_3	1	1	−2	$Np(CH_3COO)(OH)_2^+$	3.86 ± 0.03
CH_3	6	1	−12	$Np_6(\mu\text{-}CH_3COO)_{12}(\mu_3\text{-}O)_4(\mu_3\text{-}OH)_4$	52.0 ± 0.7

[a]Stability constants at I = 0.62 M calculated by the ionic strength correction (Debye–Hückel model and specific ion interaction theory, from ref 4c).

started, the main species is already $Np(HCOO)(OH)_2^+$, and its equilibrium coupled with $Np_6(\mu\text{-}HCOO)_{12}(\mu_3\text{-}O)_4(\mu_3\text{-}OH)_4$ prevails during the experiment. Figure 5a shows the crossing point of the $Np(HCOO)(OH)_2^+$ and $Np_6(\mu\text{-}HCOO)_{12}(\mu_3\text{-}O)_4(\mu_3\text{-}OH)_4$ distribution curves at pH 1.1, which is consistent with the middle point of the spectral changes in Figure 1 (pH ~1.2). At a 10-fold higher $[Np^{IV}]_{tot}$, the $Np(HCOO)(OH)_2^+$ fraction is suppressed and the formation of $Np_6(\mu\text{-}HCOO)_{12}(\mu_3\text{-}O)_4(\mu_3\text{-}OH)_4$ is enhanced as shown in Figure 5, consistent with the EXAFS trend (Figure 3). With regard to the Np^{IV}–CH_3COO^- system, the lowest pH of the UV–vis–NIR absorption spectral series of Figure S4 of the Supporting Information is 0.52, where $Np(CH_3COO)(OH)_2^+$ is predominant as shown in Figure 6. The equilibrium governing the observed spectral changes is eq 1 (x = 1, y = 2). The promotion of formation of the hexamer with the higher $[Np^{IV}]_{tot}$ was also confirmed in this system.

It should be emphasized that the stability of $Np(RCOO)(OH)_2^+$ and the hexamers depends on the R substituent of the carboxylate. With regard to the monomeric dihydrolyzed species, the difference in complex stability can be assessed using the following relationship.

$$Np(CH_3COO)(OH)_2^+ + HCOO^- = Np(HCOO)(OH)_2^+ + CH_3COO^- \quad (4)$$

The logarithmic equilibrium constant is −1.35. Although eq 4 seems to indicate $Np(CH_3COO)(OH)_2^+$ is more stable than $Np(HCOO)(OH)_2^+$, it is also necessary to take the protonation of the carboxylates into account, because $RCOO^-$ is fully protonated in substance under the actual condition for which $Np(RCOO)(OH)_2^+$ is predominant. Therefore, eq 4 is modified as follows.

$$Np(CH_3COO)(OH)_2^+ + HCOOH = Np(HCOO)(OH)_2^+ + CH_3COOH \quad (5)$$

The logarithmic equilibrium constant is −0.34, proving the stability of $Np(HCOO)(OH)_2^+$ is lower than that of $Np(CH_3COO)(OH)_2^+$.

In the next step, we assume the full replacement of the carboxylates in the hexamers as given by eq 6.

$$Np_6(\mu\text{-}CH_3COO)_{12}(\mu_3\text{-}O)_4\text{-}(\mu_3\text{-}OH)_4 + 12\,HCOO^- = Np_6(\mu\text{-}HCOO)_{12}(\mu_3\text{-}O)_4(\mu_3\text{-}OH)_4 + 12CH_3COO^- \quad (6)$$

The logarithmic constant of eq 6 is −9.30. Taking the protonation of $RCOO^-$ into consideration, we obtain eq 7.

$$Np_6(\mu\text{-}CH_3COO)12(\mu_3\text{-}O)_4(\mu_3\text{-}OH)_4 + 12\,HCOOH = Np_6(\mu\text{-}HCOO)_{12}(\mu_3\text{-}O)_4(\mu_3\text{-}OH)4 + 12CH_3COOH \quad (7)$$

Its equilibrium constant on the log scale is 2.81. This conversion from eq 6 to eq 7 is reasonable because it is obvious from Figures 5 and 6 and the log $\beta_{0,1,-1}$ values of both $RCOO^-$ groups in Table 2 that the formation of $Np_6(\mu$-

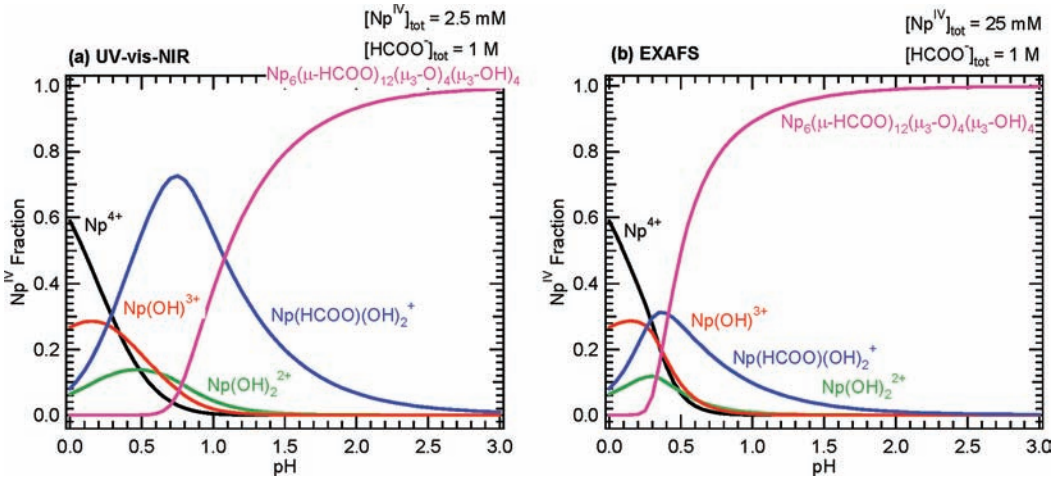

Figure 5. Speciation diagrams as a function of the pH calculated from the stability constants of species occurring in the Np^{IV}–$HCOO^-$ system under the experimental conditions for (a) UV–vis–NIR (Figure 1; $[Np^{IV}]_{tot}$ = 2.5 mM, and $[HCOO^-]_{tot}$ = 1.00 M) and (b) EXAFS (Figure 3; $[Np^{IV}]_{tot}$ = 25 mM, and $[HCOO^-]_{tot}$ = 1.00 M).

dx.doi.org/10.1021/ic201482n | Inorg. Chem. 2012, 51, 1336–1344

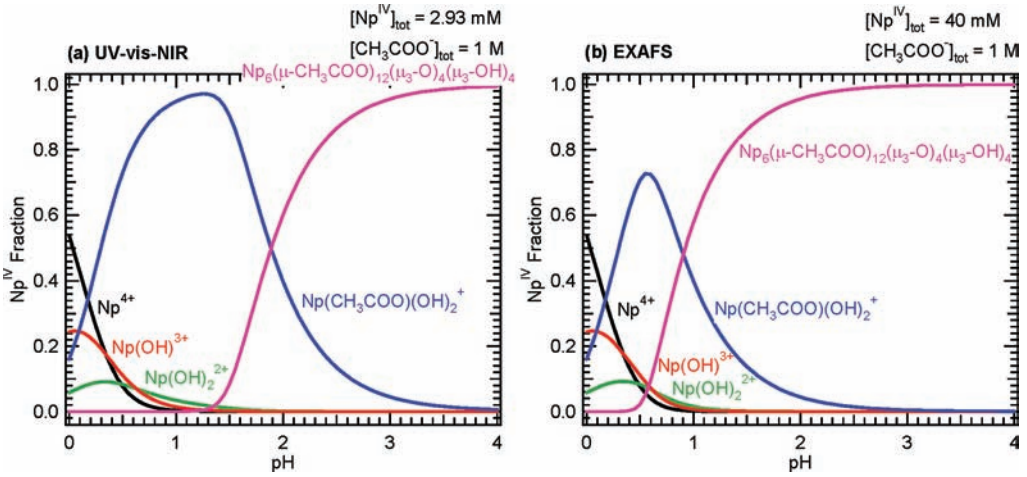

Figure 6. Speciation diagrams as a function of pH calculated from the stability constants of species occurring in the Np^{IV}–CH_3COO^- system under the experimental conditions for (a) UV–vis–NIR (Figure S6 of the Supporting Information; $[Np^{IV}]_{tot}$ = 2.93 mM, and $[HCOO^-]_{tot}$ = 1.00 M) and (b) EXAFS (Figure S7 of the Supporting Information; $[Np^{IV}]_{tot}$ = 40 mM, and $[HCOO^-]_{tot}$ = 1.00 M).

Table 3. Structural Parameters from an EXAFS Curve Fit for $Np_6(\mu\text{-aa})_{12}(\mu_3\text{-O})_4(\mu_3\text{-OH})_4$[a]

	aa^- = gly^-			aa^- = L-ala^-			aa^- = L-cys^-		
shell[b]	*N*	*R* (Å)	σ^2 (Å^2)	*N*	*R* (Å)	σ^2 (Å^2)	*N*	*R* (Å)	σ^2 (Å^2)
O_O	2.2	2.22	0.0039	2.3	2.22	0.0040	2.1	2.22	0.0042
O_C/O_{OH}	6.5	2.42	0.0070	6.7	2.42	0.0072	6.4	2.43	0.0076
C_C	3.9	3.43	0.0049	3.9	3.43	0.0050	3.6	3.45	0.0060
Np_n	3.9	3.81	0.0050	3.8	3.82	0.0049	3.9	3.83	0.0057
Np_t	1.2	5.39	0.0063	1.2	5.41	0.0078	1.0	5.42	0.0047
	ΔE_0 = −2.9 eV; *R*-factor = 0.03771			ΔE_0 = −2.9 eV; *R*-factor = 0.05043			ΔE_0 = −0.6 eV; *R*-factor = 0.02982		

[a] σ^2, Debye–Waller factor; ΔE_0, threshold energy shift. [b] Atomic notation follows Figure 4.

$RCOO)_{12}(\mu_3\text{-O})_4(\mu_3\text{-OH})_4$ occurs in the pH range where RCOOH is still predominant. The positive constant of eq 7 reveals a stability of $Np_6(\mu\text{-HCOO})_{12}(\mu_3\text{-O})_4(\mu_3\text{-OH})_4$ much higher than that of $Np_6(\mu\text{-CH}_3\text{COO})_{12}(\mu_3\text{-O})_4(\mu_3\text{-OH})_4$, although in reality the formation of mixed carboxylate hexamers like $Np_6(\mu\text{-HCOO})_i(\mu\text{-CH}_3\text{COO})_{12-i}(\mu_3\text{-O})_4(\mu_3\text{-OH})_4$ ($1 \leq i \leq 11$) also has to be taken into account.

2.4. Amino Acids. To expand our studies of the coordination of Np^{IV} to more biologically relevant ligands, α-amino carboxylic acids (amino acids, Haa) were investigated. It is also unknown how their terminal functionalities, NH_2 and the residual groups, interact or affect Np^{IV} coordination. The UV–vis–NIR absorption spectra of Np^{IV} (2.0×10^{-3} M) with glycine (Hgly, 2.02 M) were studied at various pH values. As a result, all the spectra recorded at pH 0.61–3.25 (Figure S10 of the Supporting Information) are quite similar to those of $Np_6(\mu\text{-RCOO})_{12}(\mu_3\text{-O})_4(\mu_3\text{-OH})_4$ mentioned above in Figure 1 and Figure S4 of the Supporting Information, and there seems to be no remarkable dependence on pH. This means that the Np^{IV}–Hgly hexamer is significantly formed in all test solutions. The same trend was also observed in the cases of L-alanine (0.54 M Hala, pH 2.16) and L-cysteine (0.53 M Hcys, pH 4.04) instead of Hgly [$[Np^{IV}]_{tot} = 2.5 \times 10^{-2}$ M (Figure S11 of the Supporting Information)]. To obtain evidence of formation of the hexamer in the Np^{IV}–Haa systems, the Np L_{III}-edge EXAFS experiments were performed. The results are shown in Figure S12 of the Supporting Information. All the k^3-weighted EXAFS spectra of the Np^{IV} sample solutions of Figure S11 of the Supporting Information are quite similar to each other and also to those of $Np_6(\mu\text{-RCOO})_{12}(\mu_3\text{-O})_4(\mu_3\text{-OH})_4$ (R = H or CH_3). The structural parameters evaluated from the EXAFS curve fits on the model of Figure 4 are listed in Table 3 and also are in good agreement with those of the former M^{IV}–$RCOO^-$ hexamers [M = Th, U, or Np; R = H or CH_3 (Table 1)]. In conclusion, $Np_6(\mu\text{-RCOO})_{12}(\mu_3\text{-O})_4(\mu_3\text{-OH})_4$ (the total charge of the complex will be discussed later) is formed in each Np^{IV}–Haa system. Although Haas possess their own residual functional groups, e.g., CH_3 for Hala and CH_2SH for Hcys, there seem to be no significant effects of these substituents on the hexamer core structures at first glance over the EXAFS *R* spaces depicted in Figure 3 and Figures S7, S9, and S12 of the Supporting Information.

The fact that hexamer formation is already complete at pH 0.61 when $[Np^{IV}]_{tot} = 2.00 \times 10^{-3}$ M and $[Hgly]_{tot}$ = 2.02 M (Figure S10 of the Supporting Information) is indicative of the very high stability of the Np^{IV}–Hgly hexamer. This is probably related to the unique protonation and deprotonation behavior of Haa

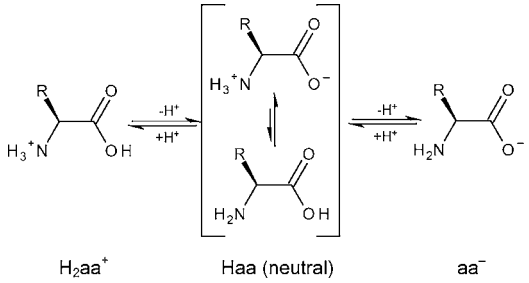

(8)

Because of the zwitterion form, the carboxylic group of Haa is already deprotonated even in the neutral state, facilitating the

dx.doi.org/10.1021/ic201482n | Inorg. Chem. 2012, 51, 1336–1344

stronger coordination of Haa to Np^{4+}. Consequently, the stability of the Np^{IV}–Haa hexamers would be advanced. Here we wonder whether the terminal quaternary ammonium group of the zwitterionic Haa is held even in the hexamers. If so, the total charge of the hexameric complex is +12 at its maximum. Although it is difficult to count the number of protonations on the amino group, the noncharged $Np_6(\mu\text{-aa})_{12}(\mu_3\text{-O})_4(\mu_3\text{-OH})_4$ (i.e., Haa is deprotonated, and aa^- acts as an anionic bridging ligand in a manner similar to that of $RCOO^-$ groups studied above) could be convincing, because the $Np-O_{O/OH/C}$ bond distances from the EXAFS fits (Table 3) are very similar to those of $Np_6(\mu\text{-RCOO})_{12}(\mu_3\text{-O})_4(\mu_3\text{-OH})_4$ [R = H or CH_3 (Table 1)]. Because of the strong tendency to form the hexamer, the detailed thermodynamics of Np^{IV}–Haa systems are not clarified at present.

3. CONCLUSION

In this study, we investigate the complexation of $RCOO^-$ (R = H, CH_3, or $CHR'NH_2$; R′ = H, CH_3, or CH_2SH) to Np^{4+} in moderately acidic aqueous solutions by using UV–vis–NIR and X-ray absorption spectroscopy. In all the cases of $RCOO^-$, water-soluble ternary hexanuclear complexes consisting of Np^{4+}, $RCOO^-$, and OH^-/O^{2-}, $Np_6(\mu\text{-RCOO})_{12}(\mu_3\text{-O})_4(\mu_3\text{-OH})_4$, were found under the higher-pH condition that was examined. The structural information for $Np_6(\mu\text{-RCOO})_{12}(\mu_3\text{-O})_4(\mu_3\text{-OH})_4$ molecules was obtained from the EXAFS curve fit and consistent with the previous reports about the similar hexanuclear complexes of Th^{IV} and U^{IV}.[11] By virtue of the stronger tendency of Np^{IV} toward its hydrolysis and hexamer formation in comparison to Th^{IV} and U^{IV}, the stability constants of $Np_6(\mu\text{-RCOO})_{12}(\mu_3\text{-O})_4(\mu_3\text{-OH})_4$ (R = H or CH_3) and the related monomer, $Np(RCOO)(OH)_2^+$, were determined from the UV–vis–NIR titration experiments. The similarity in the $M_6(\mu\text{-RCOO})_{12}(\mu_3\text{-O})_4(\mu_3\text{-OH})_4$ formation of the neighboring tetravalent early actinide elements, as well as its stability increasing with atomic number, allows us to postulate that Pu^{IV} might form $Pu_6(\mu\text{-RCOO})_{12}(\mu_3\text{-O})_4(\mu_3\text{-OH})_4$ in aqueous solution, with a stability even higher than that of Np^{IV}. In the absence of terminating ligand(s), growth of the hydrolyzed polynuclear actinide(IV) particle makes it colloidal, and it finally precipitated. Such growth of actinide(IV) hydrous oxide particles may be terminated by additional ligand(s) like $RCOO^-$ that are abundant in the natural environments, which triggers solubilization of actinide(IV) into water such as that in aquifers and promotion of their mobility in the geosphere. Recently, Soderholm and co-workers found $[Pu_{38}O_{56}Cl_{54}(H_2O)_8]^{14-}$ bearing the core structure of poorly crystalline PuO_2, of which the growth was interrupted by Cl^- decollation on the surface of the Pu_{38} cluster.[15] The influence of different ligands like Cl^- and NO_3^- on the size of such nanoparticles has also been shown by Kemner and co-workers.[16]

4. EXPERIMENTAL SECTION

Caution! *Neptunium 237 is a radioactive isotope ($T_{1/2}$ = 2.14 × 10^6 years) and an α-emitter. It has to be handled in dedicated facilities with appropriate equipment for radioactive materials to avoid health risks caused by radiation exposure. Perchloric acid and its salts are potentially explosive. Although we have not faced any serious problems so far, handling of all compounds with ClO_4^- should be done with great care and in small amounts.*

Sample Preparation. Neptunium 237 from CEA-Marcoule was purified via precipitation by alkalization and column chromatography with an anion-exchange resin (Dowex 1X8) in aqueous HNO_3. The collected fraction of purified neptunium was heated until dryness, and the residue was dissolved in 1.0 M aqueous $HClO_4$. All neptunium was again precipitated by alkalization, followed by repeated centrifugation and washing with water until the supernatant became pH neutral (five cycles, at least). The black neptunium hydroxide/oxide was dissolved in 1.0 M aqueous $HClO_4$, which was used as a stock solution of Np, in which the oxidation state of Np was a mixture of +5 and +6. The total neptunium concentration was spectrophotometrically determined. Np^{4+} was prepared by electrochemical or chemical reduction in a solution via dilution of the $Np^{V/VI}$ stock solution with water and/or 1.0 M aqueous $HClO_4$. In the former method, the sample solution with the desired concentration of $Np^{V/VI}$ was electrolyzed at −0.30 V versus Ag/AgCl, followed by bubbling air to oxidize partially generated Np^{III} to Np^{IV}. In the latter procedure, monohydrated hydrazine was used as a reducing agent. The mixture of $Np^{V/VI}$ and hydrazine was heated on a hot plate until the mixture was dry, followed by dissolving the residue in 0.20 M aqueous $HClO_4$ (1.3 mL). The pH values of the sample solutions were adjusted by adding 25 wt % aqueous NH_3. The ionic strengths of the sample solutions in the Np^{IV}–$HCOO^-$ and Np^{IV}–CH_3COO^- systems were kept at 0.62 and 0.66 M $(H,NH_4)ClO_4$, respectively. The carboxylic acids (HCOOH, Merck, 99.8–100.2%; CH_3COOH, Merck, glacial, 99.8–100.2%; glycine, Merck, ≥99%; L-alanine, Merck, ≥99%; L-cysteine, Merck, ≥99%) were used as received.

Methods. UV–vis–NIR absorption spectra were recorded by using Varian Cary 5G or J&M TIDAS 100 spectrophotometers. All measurements were taken at 295 ± 1 K.

X-ray absorption fine structure (XAFS) spectroscopy was performed at Rossendorf Beamline (ROBL) BM20 at the European Synchrotron Radiation Facility (ESRF, 6 GeV, 160–200 mA).[17] A Si(111) double-crystal monochromator was employed in channel-cut mode to monochromatize a white X-ray beam from the synchrotron. Neptunium L_{III}-edge X-ray absorption spectra of solution samples with Np^{IV} and RCOOH at different pH values were recorded in transmission mode by using argon-filled ionization chambers at ambient temperature (295 ± 1 K) and pressure. The X-ray energy in each experimental run was calibrated with a Y foil placed after the sample (first inflection point at 17038 eV). The XAFS spectrum of each sample was recorded twice and merged. EXAFS data extraction and fits were processed with IFEFFIT.[18] The threshold energy E_0 of the Np L_{III} edge was defined at 17625 eV. The curve fit was perfomed with *R* space, using phases and amplitudes calculated with *FEFF8.20*[19] based on the crystal structure of $[Th_6(\mu_3\text{-O})_4(\mu_3\text{-OH})_4(HCOO)_{12}(H_2O)_6]Na_3(ClO_4)_{3.5}(H_2O)_{5.5}(H_3O)_{0.5}$.[11a] The amplitude reduction factor S_0^2 was fixed to 0.9, and the shifts in threshold energy ΔE_0 were constrained to be the same for all included shells.

■ ASSOCIATED CONTENT

Supporting Information

Some details of the equilibrium calculations; UV–vis–NIR absorption spectra of Np^{IV} (i) with $HCOO^-$/HCOOH at different pH values, (ii) in the presence and absence of $HCOO^-$/HCOOH at pH 0.64, (iii) at different $[HCOO^-]_{tot}$ values, (iv) in EXAFS samples of Figure 3, (v) with CH_3COO^-/CH_3COOH at different pH values, (vi) at different $[CH_3COO^-]_{tot}$ values, (vii) with Hgly at different pH values, and (viii) with different amino acids; k^3-weighted Np L_{III}-edge EXAFS spectra and their FTs of Np^{IV} (i) with $HCOO^-$/HCOOH at pH 2.43 together with the best fit curves, (ii) with CH_3COO^-/CH_3COOH at different pH values, (iii) with CH_3COO^-/CH_3COOH at pH 3.02 together with the best fit curves, and (iv) with amino acids; and a table listing molar absorptivities and gross stability constants of $Np(RCOO)(OH)_2^+$ ($\beta_{1,1,-2}$). This material is available free of charge via the Internet at http://pubs.acs.org.

dx.doi.org/10.1021/ic201482n | *Inorg. Chem.* 2012, 51, 1336–1344

AUTHOR INFORMATION

Corresponding Author

*E-mail: k.takao@st.seikei.ac.jp (K.T.), hennig@esrf.fr (C.H.).

ACKNOWLEDGMENTS

S.T. was supported by a stipend from the Alexander von Humboldt foundation. This work was supported by the Deutsche Forschungsgemeinschaft under Contract HE2297/2-2.

REFERENCES

(1) (a) David van Horn, J.; Huang, H. *Coord. Chem. Rev.* **2006**, *250*, 765−775. (b) Szabo, Z.; Toraishi, T.; Vallet, V.; Grenthe, I. *Coord. Chem. Rev.* **2006**, *250*, 784−815.

(2) (a) Kaltsoyannis, N.; Scott, P. *The f elements*; Oxford University Press Inc.: New York, 1999. (b) Cotton, S. *Lanthanide and Actinide Chemistry*; John Wiley & Sons, Ltd.: Chichester, U.K., 2006.

(3) (a) Harrison, J. J.; Thyne, G. D. *Geochim. Cosmochim. Acta* **1992**, *56*, 565−586. (b) Marley, N. A.; Gaffney, J. S.; Orlandini, K. A.; Cunningham, M. M. *Environ. Sci. Technol.* **1993**, *27*, 2456−2461. (c) Nowack, B. *Environ. Sci. Technol.* **2002**, *36*, 4009−4016. (d) Schmeide, K.; Sachs, S.; Budner, M.; Reich, T.; Heise, K. H.; Bernhard, G. *Inorg. Chim. Acta* **2003**, *351*, 133−140. (e) Sutton, R.; Sposito, G. *Environ. Sci. Technol.* **2005**, *39*, 9009−9015. (f) Schmeide, K.; Reich, T.; Sachs, S.; Bernhard, G. *Inorg. Chim. Acta* **2006**, *359*, 237−242. (g) Van Riemsdijk, W. H.; Koopal, L. K.; Kinniburgh, D. G.; Benedetti, M. F.; Weng, L. *Environ. Sci. Technol.* **2006**, *40*, 7473−7480. (h) Kremleva, A.; Krueger, S.; Roesch, N. *Inorg. Chim. Acta* **2009**, *362*, 2542−2550.

(4) (a) Grenthe, I.; Fuger, J.; Konings, R. J. M.; Lemire, R. J.; Muller, A. B.; Nguyen-Trung, C.; Wanner, H. *Chemical Thermodynamics of Uranium*; OECD/NEA and North-Holland: Amsterdam, 1992. (b) Lemire, R. J.; Fuger, J.; Spahiu, K.; Nitsche, H.; Sullivan, J. C.; Ullman, W. J.; Potter, P.; Vitorge, P.; Rand, M. H.; Wanner, H.; Rydberg, J. *Chemical Thermodynamics of Neptunium and Plutonium*; OECD/NEA and North-Holland Elsevier Science B.V.: Amsterdam, 2001. (c) Fanghänel, T.; Neck, V.; Fuger, J.; Palmer, D. A.; Grenthe, I.; Rand, M. H. *Update on the Chemical Thermodynamics of Uranium, Neptunium, Plutonium, Americium and Technetium*; Elsevier Science B.V.: Amsterdam, 2003. (d) Martell, A. E.; Smith, R. M. NIST Critically Selected Stability Constants of Metal Complexes; *NIST Standard Reference Database 46*, version 8.0; Motekaitis, R. J., Developer; distributed by NIST Standard Reference Data, 2004.

(5) (a) Neck, V.; Kim, J. I. *Radiochim. Acta* **2001**, *89*, 1−16. (b) Neck, V.; Kim, J. I.; Seidel, B. S.; Marquardt, C. M.; Dardenne, K.; Jensen, M. P.; Hauser, W. *Radiochim. Acta* **2001**, *89*, 439−446.

(6) Benedict, M.; Pigford, T. H.; Levi, H. W. *Nuclear Chemical Engineering*, 2nd ed.; McGraw-Hill, Inc.: New York, 1981.

(7) Casellato, U.; Vigato, P. A.; Vidali, M. *Coord. Chem. Rev.* **1978**, *26*, 85−159.

(8) (a) Day, R. A. Jr.; Stoughton, R. W. *J. Am. Chem. Soc.* **1950**, *72*, 5662−5666. (b) Portanova, R.; Tomat, G.; Cassol, A.; Magon, L. *J. Inorg. Nucl. Chem.* **1972**, *34*, 1685−1690. (c) Tedesco, P. H.; Anon, M. C. *J. Inorg. Nucl. Chem.* **1972**, *34*, 2271−2276. (d) Portanova, R.; Di Bernardo, P.; Traverso, O.; Mazzocchin, G. A.; Magon, L. *J. Inorg. Nucl. Chem.* **1975**, *37*, 2177−2179. (e) Moore, R. C.; Borkowski, M.; Bronikowski, M. G.; Chen, J.; Pokrovsky, O. S.; Xia, Y.; Choppin, G. R. *J. Solution Chem.* **1999**, *28*, 521−531.

(9) Patil, S. K.; Ramakrishna, V. V.; Ramaniah, M. V. *Coord. Chem. Rev.* **1978**, *25*, 133−178.

(10) (a) Traishi, T.; Farkas, I.; Szabo, Z.; Grenthe, I. *J. Chem. Soc., Dalton Trans.* **2002**, 3805−3812. (b) Toraishi, T.; Grenthe, I. *Dalton Trans.* **2003**, 1634−1640.

(11) (a) Takao, S.; Takao, K.; Kraus, W.; Emmerling, F.; Scheinost, A. C.; Bernhard, G.; Hennig, C. *Eur. J. Inorg. Chem.* **2009**, 4771−4775. (b) Knope, K. E.; Wilson, R. E.; Vasiliu, M.; Dixon, D. A.; Soderholm, L. *Inorg. Chem.* **2011**, *50*, 9696−9704.

(12) (a) Lundgren, G. *Ark. Kemi* **1952**, *5*, 421−428. (b) Duval, P. B.; Burns, C. J.; Buschmann, W. E.; Clark, D. L.; Morris, D. E.; Scott, B. L. *Inorg. Chem.* **2001**, *40*, 5491−5496. (c) Nocton, G.; Burdet, F.; Pecaut, J.; Mazzanti, M. *Angew. Chem., Int. Ed.* **2007**, *46*, 7574−7578. (d) Berthet, J. C.; Thuery, P.; Ephritikhine, M. *Chem. Commun.* **2005**, 3415−3417. (e) Morkry, L. M.; Dearn, N. S.; Carrano, C. J. *Angew. Chem., Int. Ed.* **1996**, *35*, 1497−1498. (f) Nocton, G.; Pecaut, J.; Filinchuk, Y.; Mazzanti, M. *Chem. Commun.* **2010**, *46*, 2757−2759. (g) Mougel, V.; Biswas, B.; Pecaut, J.; Mazzanti, M. *Chem. Commun.* **2010**, *46*, 8648−8650. (h) Biswas, B.; Mougel, V.; Pecaut, J.; Mazzanti, M. *Angew. Chem., Int. Ed.* **2011**, *123*, 5863−5866.

(13) (a) Katz, J. J.; Seaborg, G. T.; Morss, L. R. *The Chemistry of the Actinide Elements*, 2nd ed.; Chapman and Hall: London, 1986. (b) Sjoblom, R.; Hindman, J. C. *J. Am. Chem. Soc.* **1951**, *73*, 1744−1751. (c) Waggener, W. C. *J. Phys. Chem.* **1958**, *62*, 382−383.

(14) Rossberg, A.; Reich, T.; Bernhard, G. *Anal. Bioanal. Chem.* **2003**, *376*, 631−638.

(15) Soderholm, L.; Almond, P. M.; Skanthakumar, S.; Wilson, R. E.; Burns, P. C. *Angew. Chem., Int. Ed.* **2008**, *47*, 298−302.

(16) Kemner, K. M.; Boyanov, M. I.; Eng, P.; Fenter, P.; Heald, S.; Lai, B.; Lee, S. S.; Scheckel, K. G.; Skanthakumar, S.; Soderholm, L.; Sutton, S. R.; Wilson, R. E. *Synchrotron Radiat. News* **2010**, *23*, 20−27.

(17) Reich, T.; Bernhard, G.; Geipel, G.; Funke, H.; Hennig, C.; Rossberg, A.; Matz, W.; Schell, N.; Nitsche, H. *Radiochim. Acta* **2000**, *88*, 633−637.

(18) Ravel, B.; Newville, M. *J. Synchrotron Radiat.* **2005**, *12*, 537−541.

(19) Ankudinov, A. L.; Ravel, B.; Rehr, J. J.; Conradson, S. D. *Phys. Rev. B* **1998**, *58*, 7565−7576.